Published online July 29, 2005

Nucleic Acids Research, 2005, Vol. 33, No. 13 ***4265–4275***
doi:10.1093/nar/gki731

An atypical RNA pseudoknot stimulator and an upstream attenuation signal for −1 ribosomal frameshifting of SARS coronavirus

Mei-Chi Su, Chung-Te Chang, Chiu-Hui Chu[1], Ching-Hsiu Tsai[1] and Kung-Yao Chang*

Graduate Institute of Biochemistry and [1]Graduate Institute of Biotechnology, National Chung-Hsing University, 250 Kuo-Kung Road, Taichung, 402 Taiwan

Received March 7, 2005; Revised May 16, 2005; Accepted July 6, 2005

ABSTRACT

The −1 ribosomal frameshifting requires the existence of an *in cis* RNA slippery sequence and is promoted by a downstream stimulator RNA. An atypical RNA pseudoknot with an extra stem formed by complementary sequences within loop 2 of an H-type pseudoknot is characterized in the severe acute respiratory syndrome coronavirus (SARS CoV) genome. This pseudoknot can serve as an efficient stimulator for −1 frameshifting *in vitro*. Mutational analysis of the extra stem suggests frameshift efficiency can be modulated via manipulation of the secondary structure within the loop 2 of an infectious bronchitis virus-type pseudoknot. More importantly, an upstream RNA sequence separated by a linker 5′ to the slippery site is also identified to be capable of modulating the −1 frameshift efficiency. RNA sequence containing this attenuation element can downregulate −1 frameshifting promoted by an atypical pseudoknot of SARS CoV and two other pseudoknot stimulators. Furthermore, frameshift efficiency can be reduced to half in the presence of the attenuation signal *in vivo*. Therefore, this *in cis* RNA attenuator represents a novel negative determinant of general importance for the regulation of −1 frameshift efficiency, and is thus a potential antiviral target.

INTRODUCTION

The −1 ribosomal frameshifting is a translational regulation mechanism adopted by a variety of viruses to synthesize two or more proteins at a fixed ratio starting with a single translation initiation site from the same open reading frame (ORF) (1–4). In response to the programmed frameshifting signals in messenger RNA (mRNA), the ribosome is induced to move one base backward in the 5′ direction, and then continues translation in the new −1 reading frame. The ratio between the two protein products from frameshifting can be determined by the frameshift efficiency of the stimulation signals and can be a key factor for the propagation of virus within the host. It has been suggested to be a potential antiviral target for the interference of viral propagation (5).

Efficient induction of eukaryotic −1 ribosomal frameshifting requires two *in cis* RNA elements (1,6). The first one is a hepta-nucleotides' slippery site sequence of X XXY YYZ, where the recoding occurs. Analysis indicated X can be any three identical nucleotides whereas Y represents three A or U, and Z is A, U or C. In addition, a downstream stimulator RNA structure located 6–7 nt away from the slippery site is also needed for efficient frameshifting. This downstream RNA stimulator is usually an H-type RNA pseudoknot in which nucleotides from a hairpin loop form base pairs with single-stranded region outside the hairpin. This leads to a topology featuring two helical stems of base pairing region (stems 1 and 2) connected by two single-stranded loops (loops 1 and 2) with a quasi-continuous RNA double-helical structure. However, not all RNA pseudoknots can stimulate −1 frameshifting and non-pseudoknot RNA element has been characterized to be responsible for inducing −1 frameshifting in HIV-1 (7,8).

The reported −1 frameshift efficiency induced by different RNA pseudoknots range from 1 to 4% for Beet western yellows virus (BWYV) in plant cells to 25 and 50% for mouse mammary tumor virus (MMTV) and avian infectious bronchitis virus (IBV), respectively, in animal cells (6,9,10). There is no clear picture to correlate frameshift efficiency with a specific RNA pseudoknot stimulator. However, it is thought that resistance of a pseudoknot against deformation by a marching ribosome can cause the elongating ribosome to pause (3,11–13). This will position the A- and P-site transfer RNAs (tRNAs) over the slippery site and, thus, increases the probability for ribosome to slip its A- and P-site tRNAs in the 5′ direction by one base and resume the translation in the new reading frame. Parameters known to affect frameshift

*To whom correspondence should be addressed. Tel: +886 4 22840468, ext 218; Fax: +886 4 22853487; Email: kychang@dragon.nchu.edu.tw

efficiency include sequence identity of the slippery site and its distance to the stimulator RNA, stability of the stimulator and interactions among the ribosome, the mRNA template and the associated tRNAs (1). Recently, the sequence identity of the spacer and the E-site tRNA have both been shown to modulate frameshift efficiency (14,15) as well. In addition, host factors have also been implicated to involve in efficiency modulation (16,17).

The severe acute respiratory syndrome (SARS) is an acute respiratory illness caused by a human coronavirus (HCV). Both SARS CoV and IBV belong to Coronaviridae (18–20). The IBV is known to use a −1 frameshifting mechanism to generate RNA-dependent RNA polymerase (RdRp) crucial for viral RNA replication. The 5′ portion of the IBV genomic RNA that encodes the RdRp contains a slippery site of the sequences UUUAAAC, and is followed by an H-type RNA pseudoknot with an in-frame stop codon embedded within stem 1 of the folded pseudoknot. An elongating ribosome will fall from the viral RNA template without synthesizing RdRp if −1 frameshifting did not occur in front of this in-frame stop codon. Therefore, defining the biologically relevant mRNA secondary structure, which can regulate the −1 frameshift efficiency of the SARS CoV, may provide useful information for anti-SARS strategy. In this work, we report the identification of an atypical RNA pseudoknot of SARS CoV as an efficient RNA stimulator in promoting −1 frameshifting *in vitro*, and explore the role of different stem regions in-frameshift efficiency determination. In addition, we will also demonstrate that particular viral RNA sequences upstream of the slippery site possess an attenuation effect on the overall −1 frameshift efficiency. It, thus, suggests that −1 ribosomal frameshifting can be attenuated by an RNA element upstream of the slippery site in addition to being promoted by a downstream RNA stimulator.

MATERIALS AND METHODS

Construction of reporter genes and mutagenesis

Plasmid encoding the gene for ORF 1ab junction region of SARS CoV, pCRII-SARS$_{12\,265–13\,653}$ was a gift from Professor Pei-Jer Chen and was used as the template for PCR cloning of the cDNA of viral RNA fragments. The p2luc reporter was a gift from Professor John Atkins at the University of Utah (21) and the pRL-SV40 vector was purchased from Promega. Forward and reverse DNA primers, respectively, carrying the SalI and BamHI restriction sites and appropriately designed annealing sequences were used for PCR amplification of the desired cDNA encoding SARS CoV viral RNAs from pCRII-SARS$_{12\,265–13\,653}$. The amplified inserts were then sub-cloned into the SalI/BamHI sites of p2luc using standard procedures and the resulting recombinant vectors were transformed into DH5α cell for the maintenance and selection by ampicillin. Frameshifting stimulator sequences of the minimal IBV and MMTV pseudoknot were chemically synthesized. They were amplified by forward and reverse primers, respectively, containing BsrGI and BsaAI site, and ligated into the BsrGI/BsaAI site (1392/1426) of restriction enzymes treated pRL-SV40 vectors.

All of the base pairing disruption and restoration mutants were constructed by using the quick-change mutagenesis kit from Stratagene according to the manufacturer's instructions. In contrast, PCR-based ligation approach with appropriate primers was used to assemble different chimera, which carried the attenuation signal (the sequences are available upon request), and will be described briefly. Initially, two complementary oligonucleotides containing the sense and the antisense sequences corresponding to the 3′ end and 5′ star region of the two fragments planned to be jointed were synthesized chemically. They were then used as forward (sense) or reverse (antisense) primers in combination with the corresponding reverse or forward primer carrying appropriate restriction sites to amplify the desired pre-jointed fragments from pCRII-SARS$_{12\,265–13\,653}$. The two individual PCR products with partially overlapping sequences were then assembled by the PCR-based ligation procedure (22), and then sub-cloned into the BamHI/EcoRI sites of p2luc vectors. The identities of all cloned and mutated genes were confirmed by DNA sequencing analysis.

RNA structure probing

RNA transcripts spanning the SARS$_{13\,377–13\,475}$ region of SARS CoV were generated by *in vitro* transcription using T7 RNA polymerase. The purified RNA of desired length was then dephosphorylated by shrimp alkaline phosphatase and 5′ end labeled with [γ-^{32}P]ATP using T4 polynucleotide kinase, and separated by a 12% sequencing gel. All the RNase protection experiments were performed in 50 μl reaction volumes containing 50 000–70 000 c.p.m. of 5′ end labeled RNA in the presence of RNase cleavage buffer (30 mM Tris–HCl, pH 7.5, 3 mM EDTA and 200 mM NaCl), and 10 mM $MgCl_2$ was included in the same buffer for RNase V1 experiments. Before the addition of probing enzymes, the RNAs were denatured by heating at 70°C for 5 min followed by instant cooling on ice and brought back to 20°C for structural mapping. The following amounts of RNases were added for each reaction: 0.0088 (1000×)–0.044 (200×) μg RNase A (USB), 0.05–10 U RNase T1 (USB), 0.5–15 U RNase T2 (USB) and 0.01–01 U RNase V1 (Amersham Pharmacia). The hydrolysis RNA ladders were obtained by the incubation of RNA in the hydrolysis buffer at 85°C for 10 min and parallel RNA sequencing products were obtained by the treatment of unfolded RNA with RNases T1 and A. They were used as markers for the assignment of guanines and pyrimidines, respectively. All the reactions were incubated at 20°C for 10 min with the exception that RNase V1 was incubated for 15 min. The reactions were terminated by phenol–chloroform extraction, and precipitated, washed with 70% ethanol, and dried by vacuum. Finally, the cleavage products were loaded into a 10% denaturing gel with different running time to resolve different parts of RNA, and visualized by using phosphorimagery.

In vitro transcription/translation and frameshift assay

The T7-coupled transcription/translation (TNT) system (Progema) was used for the generation of the shifted and the non-shifted protein products according to the manufacturer's instructions. In each assay, a 25 μl reaction containing 500 ng of DNA template, 12.5 μl of reticulocyte lysate and 0.8 μl of 10 μCi ^{35}S-labeled methionine (NEN) was incubated at 30°C for 1.5 h. The samples were then resolved by 12% SDS–PAGE and exposed to PhosphorImager screen

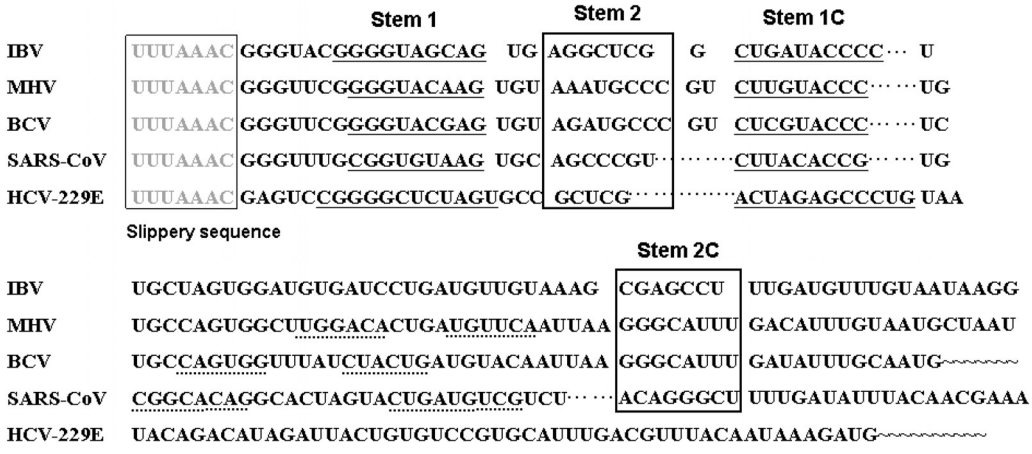

Figure 1. Characterization of the *in cis* RNA elements involved in −1 frameshifting for SARS CoV. Sequence alignment for a set of related coronaviruses. The slippery site is boxed and typed in gray, whereas the complementary base pairing counterpart of stem regions 1 and 2 (S1-S1C and S2-S2C) of stimulator are underlined and boxed by solid line, respectively. The potential base pairing scheme for the third stem (S3) is underlined by dashed line. The S2C region for HCV 229E is not shown as it appears in further downstream region.

for quantification after drying. The frameshift efficiency was calculated by dividing the counts of the shifted product by sum of the counts for both shifted and non-shifted products, with correction of the methionine number in each product. Control experiments with the plasmids of 100–1000 ng produce similar results for frameshift efficiency (data not shown). For the generation of capped mRNA templates, the mMESSAGE mMACHINE kit (Ambion) was used according to the manufacturer's instructions.

Mammalian cell culture and luciferase assay

Human embryonic kidney HEK-293T cells were cultured in the DMEM supplemented with 10% fetal bovine serum. The transient expression was performed by LIPOFECTIN (Gibco BRL) transfection of 500 ng of reporter plasmids into 12-wells cultured cells. The cells were then assayed for the transient expression of the reporter gene 24 h after transfection using dual-luciferase assay of cell lysates, and normalized by β-galactosidase activity as an internal control. All the *in vivo* experiments were repeated three times with four to six assays for each reaction. Luciferase activity measurements for both *in vitro* reticulocyte lysate and *in vivo* transfected 293T cell lysates were performed by using the dual-luciferase™ reporter assay (Promega) according to the manufacturer's instructions on an ABI TR 717 luminometer. Calculation of luciferase-based frameshift efficiency was performed with control plasmids to calibrate the ribosome drop-off effect as described previously (21).

RESULTS

The −1 frameshifting stimulator of SARS CoV contains an atypical H-type pseudoknot with an extra stem–loop in loop 2

Sequence alignment of the junction regions of ORF 1ab of SARS CoV and other coronaviruses indicated the existence of conserved UUUAAAC slippery site followed by a stretch of viral RNA sequences with the potential to form an H-type RNA pseudoknot (Figure 1). This region of the SARS CoV RNA genome, $SARS_{13\,369–13\,520}$ (for residues 13 369–13 520) was thus cloned into p2luc vector to examine its −1 frameshifting activity (21). To faithfully monitor frameshift efficiency, we also arranged the terminus of the viral sequences under investigation to keep the TAA sequences in the N-terminal part of firefly luciferase ORF in frame to act as a stop codon in the presence of −1 frameshifting. This leads to premature termination of the frameshifted product and, thus, prevents the underestimation of frameshift efficiency because this manipulation can minimize the ribosome drop-off effect while translating the full-length firefly ORF (21). A different vector, pRL-SV40 was also used as the second reporter. Frameshift assay using either of the reporters indicated that the selected viral RNA sequences possess a frameshift efficiency of 60% (data not shown), which suggests that the $SARS_{13\,369–13\,520}$ RNA contains an efficient −1 frameshifting stimulator *in vitro*.

Further examination of sequence contents of the $SARS_{13\,369–13\,520}$ RNA revealed a potential stem–loop structure within the loop 2 region of this IBV-type pseudoknot. Furthermore, their primary sequences were found to be conserved among isolated SARS CoV sequences, and similar stem–loop structures were also identified in the loop 2 region of bovine coronavirus and mouse hepatitis virus pseudoknot (Figure 1). To confirm the existence of the predicted atypical pseudoknot, enzymatic structure probing experiments were performed on $SARS_{13\,377–13\,475}$ RNA and some of the results are shown in Figure 2A. As can be seen, the distribution of cleavage patterns for ribonuclease probes sensitive to single-strand region (such as RNase T2, T1 and A in lanes 7–12 of Figure 2A) is in agreement with the existence of loop regions, whereas the cleavage pattern by RNase V1 (lanes 5 and 6) that prefers cutting of duplex and stacked conformations can be localized to the three predicted stem regions (S1, S2 and S3). However, co-existence of cleavage by both RNase V1 and single-strand sensitive probes can be found for nucleotides localized to the junction region between S2 and S3. This is probably caused by a dynamic conformational equilibrium in this region as non-denaturing gel analysis suggests that the

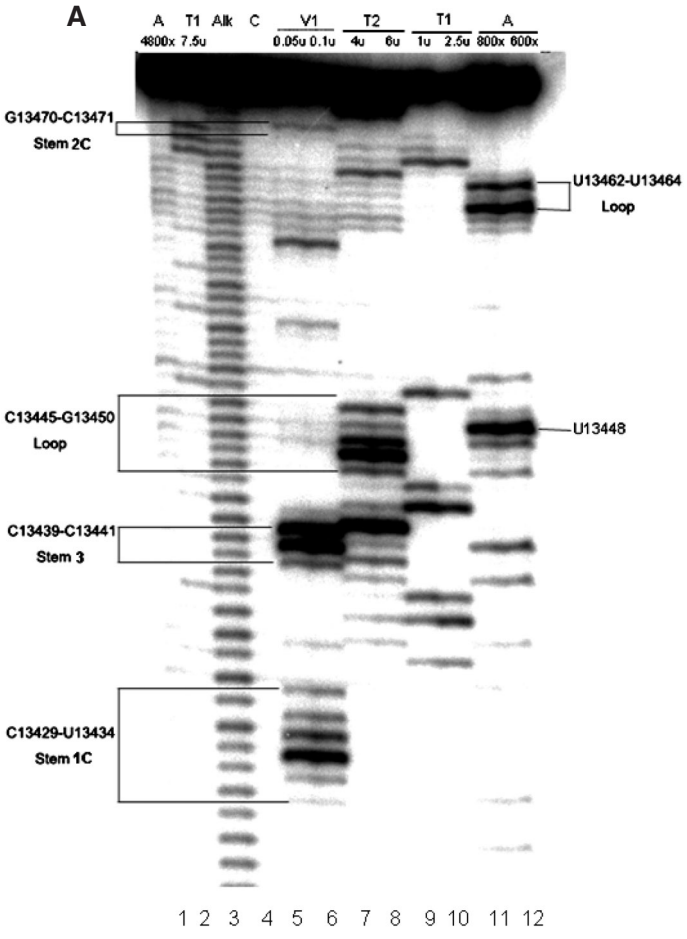

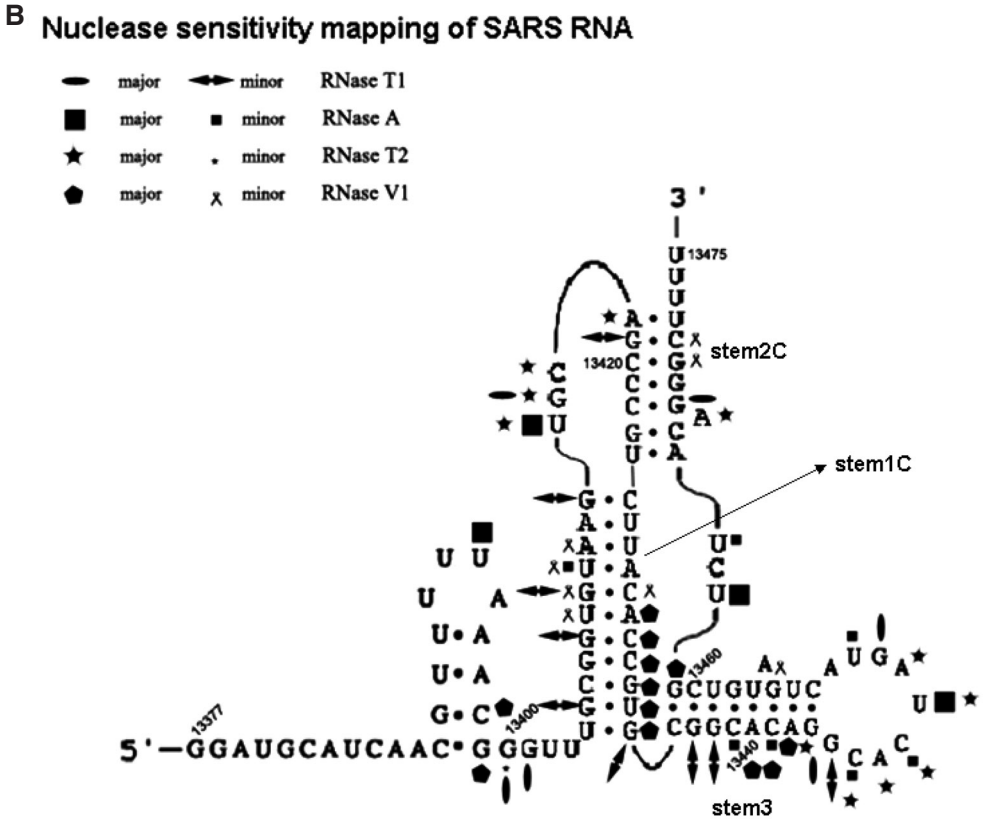

$SARS_{13\,377–13\,475}$ RNA adopts a single conformation (data not shown). Nevertheless, these probing data are consistent with the existence of a stem conformation within the loop 2 in this atypical IBV-type pseudoknot as summarized in Figure 2B. Recently, the same S3 conformation has also been proposed and verified independently (23,24).

Disruption of the base pairing region in S3 of an atypical pseudoknot impairs −1 frameshifting stimulation activity of the $SARS_{13\,369–13\,520}$ RNA. To define the contribution of different stem regions of this atypical IBV-type pseudoknot in the stimulation of −1 frameshifting activity, we mutated those nucleotides mapped onto form the duplex conformations. Mutants expected to disrupt a stem and those expect to reform the stem by compensatory base changes were then measured for their efficiency in promoting −1 frameshifting *in vitro* (Figure 3A). As shown in lanes 1–3 of Figure 3B, frameshift efficiency drops from 60% for wild-type construct to <1% for both 5′ and 3′ mutants that prevent the formation of base pairing in S1. In contrast, frameshift efficiency for the mutant with compensatory base changes to restore the base pairing scheme in S1 (lane 2 of Figure 3C) rises back to the wild-type level (55%). Similar results are observed for S2 with mutants destroying or reforming base pairs in the mapped duplex region (lanes 4 and 5 of Figure 3B and Lane 3 of Figure 3C). These experiments complement structural mapping data and strongly support the idea that it is the formation of the two typical H-type pseudoknot stems, S1 and S2, and not their sequence identities are required for efficient −1 frameshifting stimulation.

Interestingly, lower sensitivity to base pairing disruption is observed for mutants located in the mapped S3 region. Mutants with disruption of base pairing in the upper or and in the lower stem region of S3 both led to a substantial decrease in frameshift efficiency when compared with the wild-type construct (from 60 to 36 or 37%, respectively, in lanes 6 and 7 of Figure 3B). However, restoring the base pairing scheme in either portion by compensatory base changes restored frameshift efficiency to the wild-type level including the up-restoration mutant that even displays a completely different sequence composition (lanes 4 and 5 in Figure 3C), suggesting that the formation of base pairing and not the sequence contents in S3 is involved in the efficient frameshifting activity of this atypical IBV-type pseudoknot. Intriguingly, frameshift efficiency does not reduce further when more bases were mutated to disrupt all the potential base pair in S3 (lanes 8 and 9 of Figure 3B), implicating the existence of a residual frameshift activity for the remaining pseudoknot scaffold. Furthermore, a pseudoknot mutant lacking the S3 but harboring an 8 nt loop 2 possesses a frameshift efficiency of 53% (lane 10 in Figure 3B). As the topology and activity of this mutant are similar to those of the minimal IBV pseudoknot that lacks 75% of its wild-type loop 2 sequences (25), which indicates that S3 is not absolutely required for high frameshift efficiency. To rule out the possibility that the observed frameshift efficiency variation in S3 mutants is the outcome of their differences in ribosome loading efficiency of uncapped mRNA templates, separately transcribed capped mRNAs were also used to examine their *in vitro* frameshift efficiency as shown in Figure 3D. The data confirm the result from transcription-coupled translation approach used above, although lower frameshift efficiency for the wild-type construct is observed. Together, these data suggest that the roles of S3 in −1 frameshifting stimulation may be different from those of S1 to S2.

Viral RNA sequences upstream of the slippery site can downregulate −1 frameshift efficiency *in vitro*

Recently, analysis of a SARS CoV viral RNA genome containing a longer viral construct has revealed a very different frameshift efficiency from those observed in this work (26). To resolve this issue, we constructed a series of longer viral RNA-containing reporters with stepwise extension of viral insert in the 5′ direction upstream of the slippery site and measured their frameshift efficiencies. As shown in Figure 4A, frameshift efficiency of these viral RNA constructs are all lower than that of the shorter $SARS_{13\,369–13\,520}$ RNA construct. Analysis of these data suggested that the proximal 150 nt region upstream of the slippery site, that is, the sequences 13 222–13 368 possess most of the observed downregulation effect because addition of the other 475 nt further upstream of it (the sequences 13 222–12 748) only lead to a 2% decrease in frameshift efficiency (compare lane 7 with lane 3 of Figure 4A). Together, it argues that the $SARS_{13\,222–13\,368}$ viral RNA may possess a signal for the attenuation of −1 frameshift efficiency.

To confirm that the decrease in frameshift efficiency is contributed by the $SARS_{13\,222–13\,368}$ viral RNA sequence, a reporter containing a large viral insert but lacking the potential attenuation signal (sequences 13 222–13 368), $SARS_{12\,748–13\,368}\ \Delta_{att}$ was constructed. This construct possesses a frameshift efficiency of 55% although much longer protein is translated upstream of the slippery site and, thus, confirming the attenuation activity of the removed domain (compare lanes 2–4 of Figure 4B). Furthermore, the downregulation effect almost disappears for a chimera construct that has the potential attenuation signal fused downstream to the pseudoknot stimulator, arguing that this attenuation signal need to be positioned upstream of the slippery site to execute its function *in vitro* (lane 5 of Figure 4B). To examine whether the observed downregulation effect is mediated by polypeptide encoded by the viral RNA or by the RNA itself, an ORF-shifted mutant was generated and tested for its attenuation activity. In this construct, an A residue and two U residues are separately inserted into three different positions of the $SARS_{13\,222–13\,368}$ viral RNA to shift the reading frame, and consequently change the identity for 43 of the 50 amino acids encoded by the wild-type viral RNA sequences (Figure 5A). The result in Figure 5A indicates similar downregulation effect for this construct when

Figure 2. The $SARS_{13\,369–13\,520}$ RNA contains an atypical H-type pseudoknot. (**A**) Electrophoretic analysis of probing data confirms the existence of S3. The enzymatic cleavage result was resolved in a 10% sequencing gel with the first two lanes representing pyrimidines and guanine assignment markers, respectively. The third and fourth wells are alkaline hydrolysis ladder and control, respectively. The concentration of the probes used and the assignment of residues are all shown on top of the gel directly. (**B**) Summary of probing data supports the predicted S3 for an atypical H-type pseudoknot within the stimulator RNA. Extent of cleavage for each probe is defined as major or minor cut as indicated by the symbols.

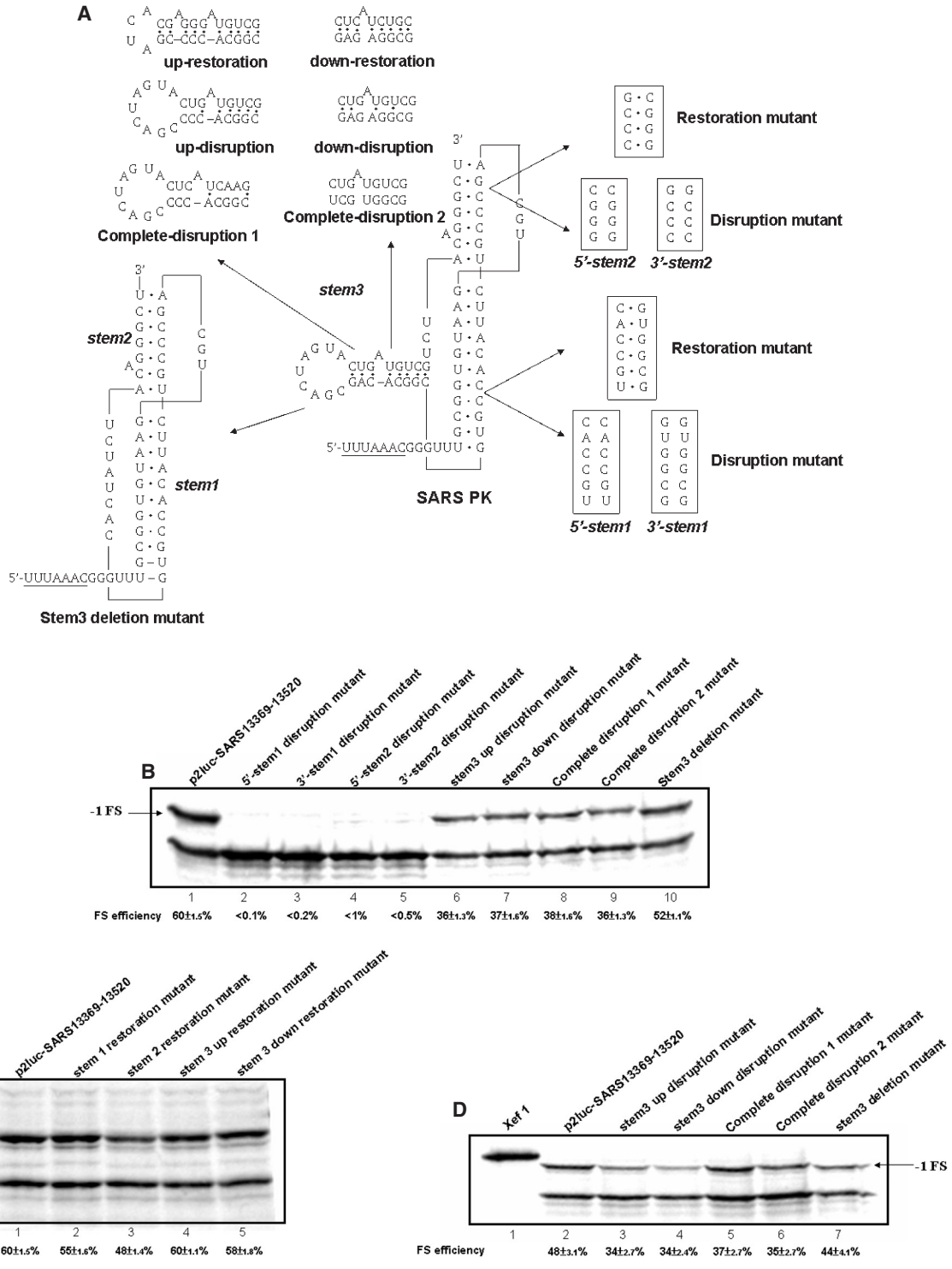

Figure 3. Role of base pairing formation in S3 may be different from those in S1 to S2 for the promotion of −1 frameshifting. (**A**) Illustration of mutant constructs for the manipulation of base pairing scheme. (**B**) Results of 12% SDS–PAGE analysis of frameshift efficiency for constructs of different base pairing scheme disruption mutants (as indicated in the top). (**C**) Results of 12% SDS–PAGE analysis of frameshift efficiency for different stem restoration constructs (as indicated in the top). (**D**) Results of 12% SDS–PAGE analysis of frameshift efficiency for different stem 3 constructs (as indicated in the top) using capped mRNA templates. The calculated efficiency is shown in the bottom of the gel and the bands of shifted product are arrowed by −1FS.

compared with the wild-type construct. Taken together, these data provide strong evidences that the upstream RNA itself as well as its orientation to the slippery site are crucial for the *cis* downregulation effect of −1 frameshift efficiency *in vitro*, and the most stable structure of $SARS_{13\,222–13\,368}$ RNA predicted by RNA structure version 4.11 (27) is presented in Figure 5B with a calculated free energy of −37.7 kcal/mol.

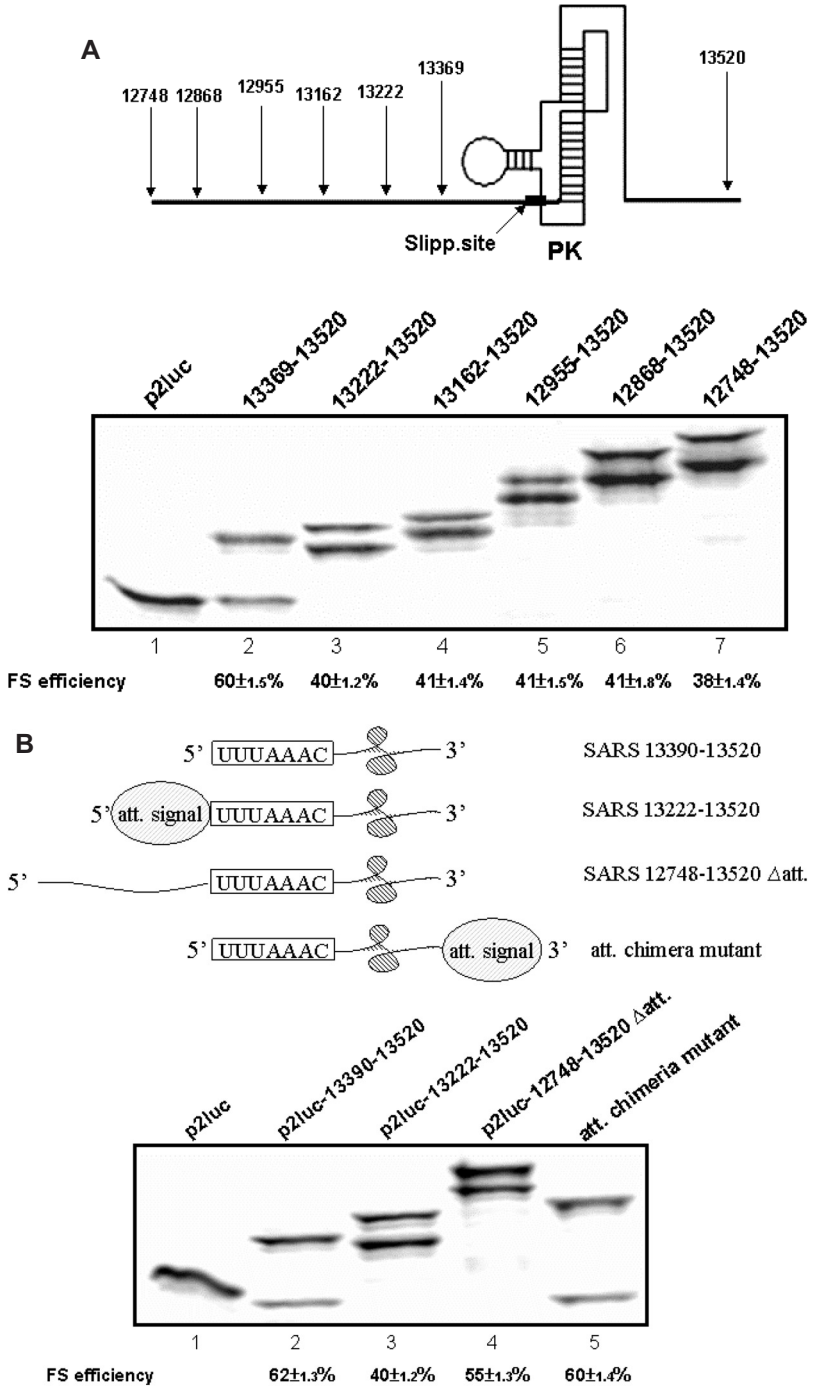

Figure 4. An RNA attenuation signal is characterized upstream of the slippery site. (**A**) Results of 12% SDS–PAGE analysis of −1 frameshifting of different upstream extension constructs with the calculated efficiency shown in the bottom of the gel. The lower and higher bands within each well belong to the shifted and the non-shifted products, respectively. The schematic diagram on top of the gel shows the relative position of the stimulator pseudoknot, the slippery site (filled box) and the extended upstream and downstream viral sequences for the constructs under analysis. (**B**) The attenuation signal need to work *in cis* and its orientation to the slippery site is crucial for its downregulation activity. Cartoons are used to illustrate the relative orientation of the attenuation signal, the slippery site and the stimulator within the inserts under analysis. The identity of insert within each reporter construct and the calculated frameshift efficiency are shown in top and bottom of the gel, respectively.

Downregulation effect of the attenuation signal is general *in vitro* and also active *in vivo*

We also evaluated the generality of downregulation effect of this attenuation signal towards other −1 frameshifting stimulators by placing it upstream of the minimal RNA pseudoknot from IBV and MMTV, respectively (25,28) (Figure 6A). Results show this upstream attenuation sequence also downregulates −1 frameshifting promoted by RNA stimulator derived from IBV and MMTV (compare

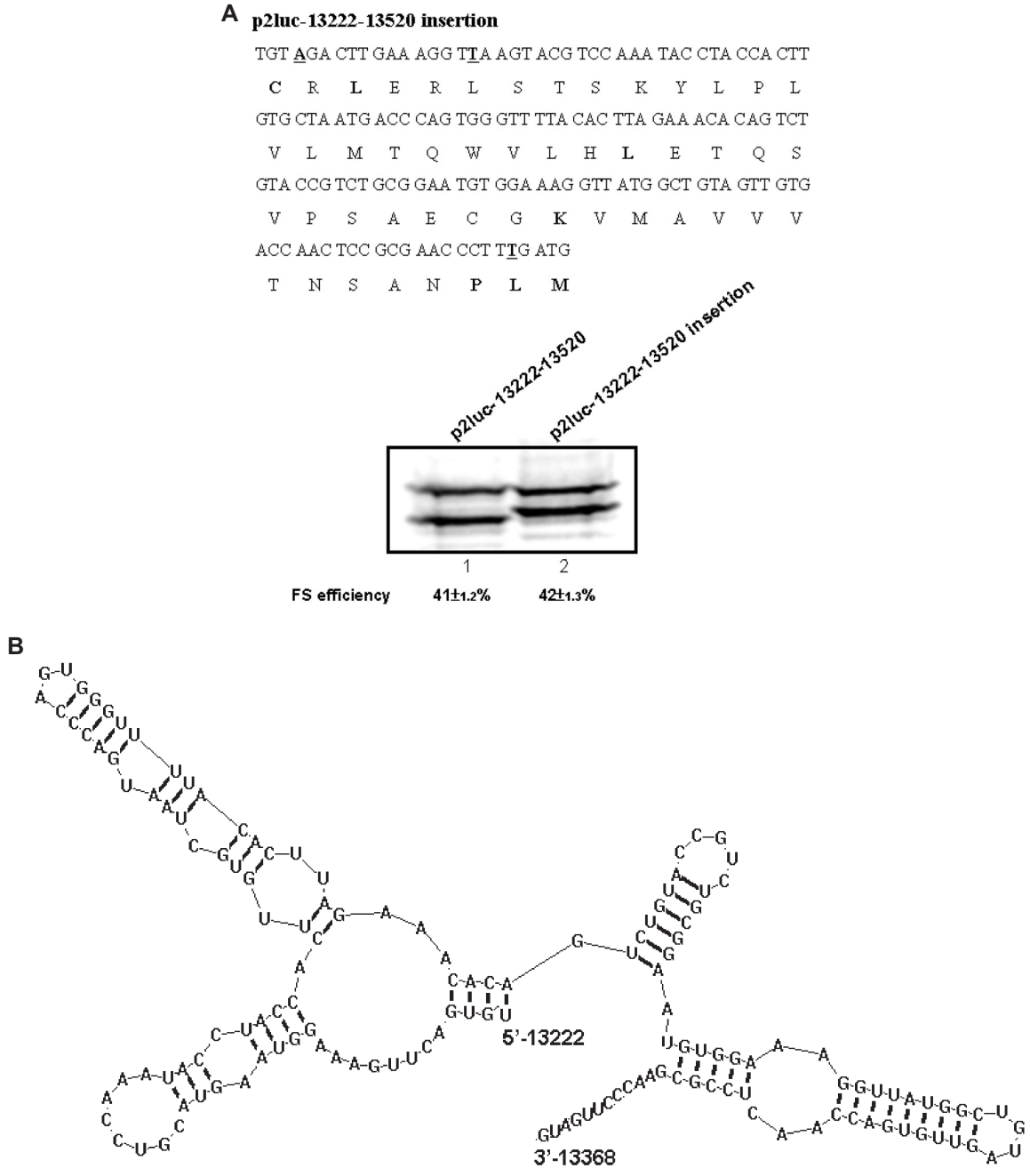

Figure 5. The $SARS_{13\,222–13\,368}$ viral RNA possesses most of the attenuation activity *in vitro*. (**A**) Changing amino acids identity encoded by $SARS_{13\,222–13\,368}$ RNA cannot abolish attenuation activity. The RNA sequences and the amino acids of polypeptide encoded by the reading frameshifted mutant are shown. The three inserted nucleotides are underlined and the encoded amino acids that remain unchanged are typed in bold face. (**B**) The most stable secondary structure of residue 13 222–13 368 RNA predicted by RNAstructure version 4.11 (27).

lanes 2–5 of Figure 6A). However, a weaker downregulation effect is observed when the attenuation signal is coupled to the minimal MMTV pseudoknot comparing with the minimal IBV pseudoknot. Therefore, the attenuation effect of this upstream signal can vary with the identity of the downstream stimulator. Finally, capped mRNA templates with or without the attenuation signal for the minimal IBV construct used above as well as a SARS viral construct carrying residues 12 265–13 652 and lacking any luciferase-related segment were also created to analyze their *in vitro* frameshift efficiencies. The results shown in Figure 6B reveal parallel results with the previous study in Figures 4A and 6A, and further rule out the involvement of ribosome loading difference in the observed attenuation effect. Furthermore, it demonstrates that such attenuation activity is not an artifact caused by the reporter system used because the inhibitory effect also functions within an all-viral context (compare lanes 2 with 3 of Figure 6B).

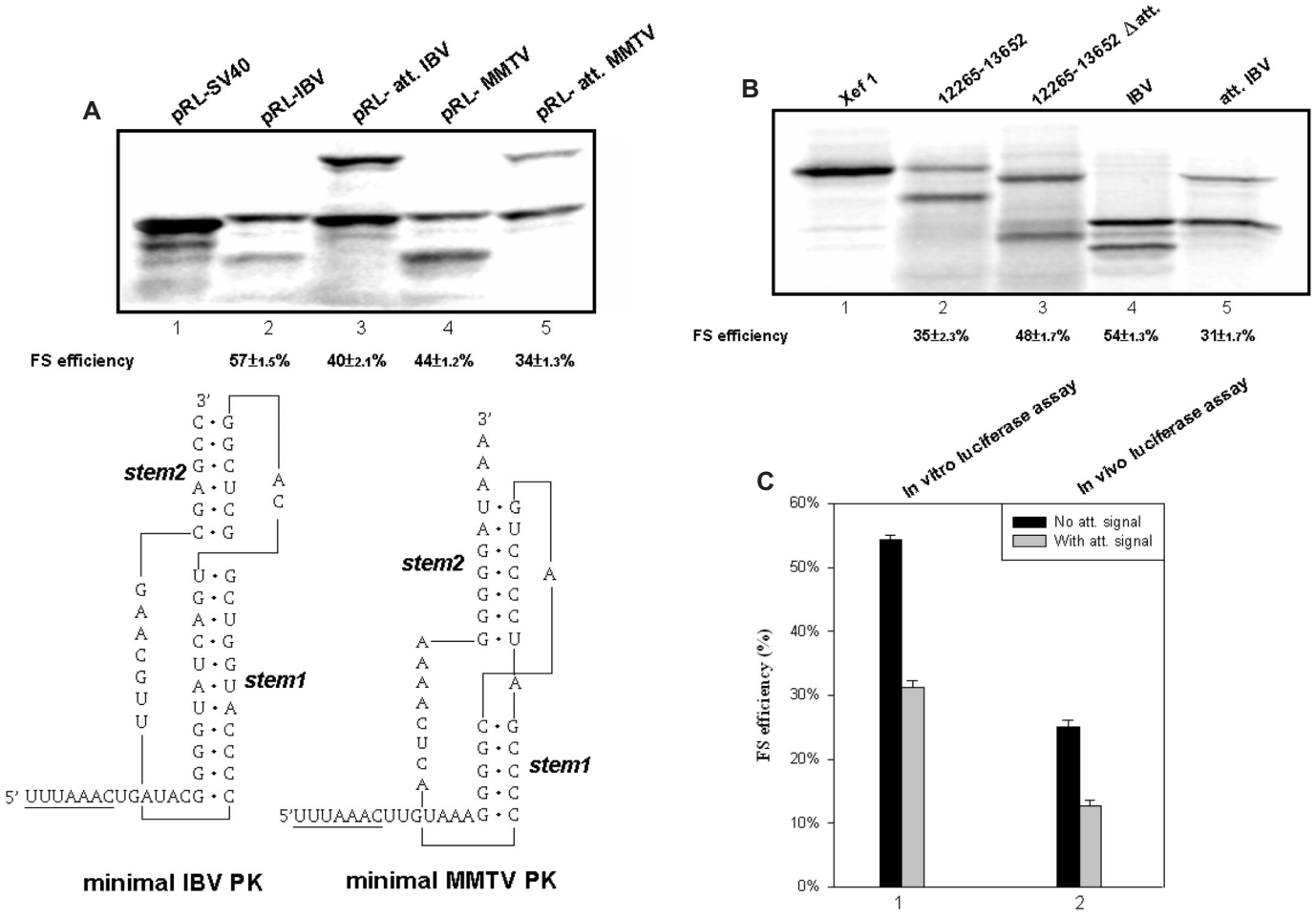

Figure 6. The general attenuation signal embedded in $SARS_{13\,222–13\,368}$ RNA is a novel negative determinant for −1 frameshifting. (**A**) The attenuation signal also downregulates −1 frameshifting promoted by other pseudoknot stimulators. In this study, the Prl-SV40 reporter was used with the insertion of minimal IBV or MMTV pseudoknot containing or lacking the upstream attenuation signal as indicated on top of the gel. The calculated frameshift efficiency is shown in the bottom of the gel. The predicted secondary structure of the minimal IBV and MMTV pseudoknot are shown in the bottom as indicated and the slippery site is underlined. (**B**) Results of 12% SDS–PAGE analysis of frameshift efficiency for capped mRNA templates. The Xef1 represents *Xenopus* elongation factor 1α protein and is used as a protein marker control. The calculated efficiency is shown in the bottom of the gel and the bands of shifted product are arrowed by −1FS in both (A) and (B). (**C**) The attenuation activity of $SARS_{13\,222–13\,368}$ RNA also functions *in vivo*. Comparison of frameshift efficiency for reporter constructs in the presence or absence of attenuation signal. The data are calculated from the results of dual-luciferase assay *in vitro* (lane 1) and *in vivo* (lane 2), respectively. The plotted values are the mean value calculated from three independent experiments with the error bars representing SD.

To evaluate the biological significance of this attenuation signal in the regulation of −1 frameshifting, we constructed several p2luc-based reporters for inserts possessing or lacking $SARS_{13\,222–13\,368}$ viral RNA without shifting the stop codon located before firefly luciferase ORF to utilize the dual-luciferase activity to monitor frameshift efficiency *in vivo* (21). The *in vitro* frameshift efficiency of these constructs were calculated from dual-luciferase assay result of the TNT products of both plasmids (lane 1 in Figure 6C), and reveals parallel results with the frameshift efficiency reported above (lanes 2 and 3 of Figure 4A). Similarly, calculation from the *in vivo* dual-luciferase assay result for cells transfected with the reporter constructs indicates that the frameshift efficiency reduces almost in half in the presence of attenuation signal comparing with the one lacking the attenuation signal (lane 2 in Figure 6C). Thus, this upstream attenuation signal also functions *in vivo*.

DISCUSSION

Manipulation of loop 2 conformation can modulate the −1 frameshift efficiency of IBV-type pseudoknot

The pseudoknot of short S1 with a bent helical junction such as the one in MMTV and the IBV-type pseudoknot of long S1 with a stringent length-requirement of 11 bp represent two distinct classes of frameshift-stimulating pseudoknot (25,28–30). In either case, the ability to resist deformation by the translocating ribosome is thought to determine the frameshift efficiency stimulated by a specific pseudoknot (8,11,13,31). Alternatively, optimal contacts between the activity in ribosome and the stimulator for its efficient unwinding may also play roles in pseudoknot-stimulated −1 frameshifting (32). The impairment of −1 frameshifting for mutants with the disruption of S1 or S2 in SARS CoV pseudoknot can be rationalized by the formation of two

separated hairpins and the coupled destruction of pseudoknot configuration. In contrast, disruption of the base pair in S3 is expected to be less important as the long loop 2 of the IBV-type pseudoknot has been thought to play a connection role to link the two stems (25). This is consistent with the wild-type like frameshift efficiency for the mutant lacking S3 in this study. Interestingly, the minimal IBV pseudoknot lacking most of its wild-type loop 2 sequences promotes −1 frameshifting better than its wild-type counterpart (10,25), whereas reverse trend is observed here for similar study on the SARS CoV pseudoknot. However, the medium frameshift efficiency for the two IBV-type mutants generated by complete base pairing disruption of S3 in SARS CoV pseudoknot suggest that the integrity of these base pairs in S3 may contribute extra −1 frameshifting activity in a delicate manner. We also note that existences of two extra base pair in the up-restoration mutants does not further enhance frameshift efficiency, implicating only a threshold value of stability is required. Taken together, they indicate that different secondary structure compositions within the loop 2 of IBV-type pseudoknot may modulate the frameshift efficiency of this type of pseudoknot, and implicate that the frameshift efficiency might be tunable by modulation of the S3 formation *in vivo*. Alternatively, the formation of S3 may also serve to prevent formation of unfavorable conformations that may interfere with frameshifting process as the long loop 2 could be merely constraint imposed by the encoded amino acids required for the RdRp activity.

The atypical pseudoknot found in this work is different from those in transmissible gastroenteritis virus (TGEV) and HCV 229E, which also contain an additional stem essential for −1 frameshifting (33,34). The additional stem of 229E pseudoknot is formed by complementary sequences between the very long loop 2 and the 3′ end sequences following stem 2, and is probably stacked onto stem 2 to form a quasi-continuous helix of 24–25 bp. In contrast, the S3 of SARS CoV pseudoknot could stack into the bottom of S1 to form a quasi-continuous helix of 25–26 bp interrupted by two separated A-bulges. Although our mapping data cannot provide information about stacking configuration among these stems in the SARS CoV pseudoknot, helical junction geometry between S1 and S2 obviously will be coupled to the positioning of S3. As modulation of frameshift efficiency by the modification of junction geometry via tertiary interactions has been observed in helical junction of BWYV pseudoknot (35,36), the modulation of helical junction configuration by the additional S3 in SARS CoV pseudoknot could also play an important role here. Furthermore, the existence of single-strand cutter cleavage for residues connecting S2 and S3 in probing data also suggests a dynamic nature of the junction region. Therefore, reduced frameshift efficiency in mutants potentially disrupting partial or all of the base pair in S3 can thus be caused by changes in junction geometry with the weakening or diminishing of S3 in these mutants.

Upstream attenuation sequence is a novel determinant for −1 frameshifting

The significant decrease in −1 frameshift efficiency by upstream attenuation signal appears unexpected as the major viral factors characterized to determine frameshift efficiency all involve sequences between the slippery site and the downstream stimulator. Interestingly, recent works on HIV-1 and barley yellow dwarf virus (BYDV) both reported the involvement of sequences upstream of the slippery site in modulation of overall −1 frameshift efficiency (37,38). However, only short sequences immediately upstream of the slippery site are involved in the case of HIV-1, and the modulation can go either way for enhancement or attenuation without a defined activity (37). In contrast, a conserved hairpin upstream of the slippery site was proposed to slow down the marching ribosome and thus enhance −1 frameshift efficiency in the case of BYDV (38). Recently, mutational study on the nucleotide adjacent to the slippery site of the SARS CoV also reported an increment of −1 frameshift efficiency *in vivo* (24). Our finding is thus unique in which, it specifies an RNA element of negatively regulatory activity with general application, and suggest that it is an integral part for the −1 frameshift efficiency determinant of SARS CoV although it is separated from the slippery site with an intervenient spacer. Although sequence alignment and secondary structure prediction for both $SARS_{13\,222–13\,368}$ and $SARS_{13\,318–13\,368}$ RNA with the corresponding regions of other coronavirues reveal no strong consensus, the sequences of $SARS_{13\,318–13\,368}$ RNA do conserve among different strains of SARS CoV (data not shown). The existence of such an attenuation signal may provide the virus a regulation point for the tuning of RdRp synthesis in response to environmental changes. In contrast, a change in spacer sequence identity will lead to a fixed frameshift efficiency although it also reduced the efficiency. Furthermore, it may also change the property of the encoded amino acid composition in the N-terminal region of RdRp with dramatic impacts on the activity of RdRp.

With respect to the mechanisms responsible for the function of this negative determinant of −1 frameshifting, the factors known to affect frameshift efficiency should be examined in the future. However, it is less possible that it is mediated by the encoded polypeptide because 14 out of 18 amino acids encoded within $SARS_{13\,318–13\,368}$ RNA were changed in the out of frame mutant and no dramatic change in attenuation activity has been observed. In contrast, it is more likely that the attenuation signal can contact with and affect the factors capable of modulating the frameshift efficiency. Indeed, interferences of dynamic interactions/contacts between pseudoknot and the ribosome or auxiliary factors in mutants of BWYV pseudoknot have been proposed to be responsible for observed frameshift efficiency variation comparing with that of its wild-type counterpart (36). However, it is tempting to speculate that the function of this attenuation element may be related to the extra S3 of downstream atypical pseudoknot. However, the fact that the attenuation signal also downregulates −1 frameshifting promoted by other stimulators suggests its function is general. Furthermore, the requirement for an orientation upstream of the slippery site and the stimulator *in vitro* indicates that function of the attenuation signal is probably not mediated via interactions with the downstream determinants of −1 frameshifting. Further biochemical analysis of the attenuation element will be informative for revealing how it works and providing insight of the mechanism of −1 ribosomal frameshifting.

ACKNOWLEDGEMENTS

We are very grateful to Dr Pei-Jer Chen for the plasmid pCRII-SARS$_{12\,265–13\,653}$, Dr John Atkin for plasmid p2Luc and Dr Hung-Wen Chen for providing cell culture facilities. This work was supported by Grant NSC 92-2751-B-005-002-Y (K.-Y.C.) and NSC 92-2751-B-005-004-Y (C.-H.T.) from the National Science Council of Taiwan. Funding to pay the Open Access publication charges for this article was provided by National Chung-Hsing University.

Conflict of interest statement. None declared.

REFERENCES

1. Farabaugh,P.J. (1996) Programmed translational frameshifting. *Microbiol. Rev.*, **60**, 103–134.
2. Gesteland,R.F. and Atkins,J.F. (1996) Recoding: dynamic reprogramming of translation. *Annu. Rev. Biochem.*, **65**, 741–768.
3. Harger,J.W., Meskauskas,A. and Dinman,J.D. (2002) An 'integrated model' of programmed ribosomal frameshifting. *Trends Biochem. Sci.*, **27**, 448–454.
4. Namy,O., Rousset,J.P., Napthine,S. and Brierley,I. (2004) Reprogrammed genetic decoding in cellular gene expression. *Mol. Cell*, **13**, 157–168.
5. Dinman,J.D., Ruiz-Echevarria,M.J. and Peltz,S.W. (1998) Translating old drugs into new treatments: ribosomal frameshifting as a target for antiviral agents. *Trends Biotechnol.*, **16**, 190–196.
6. Chamorro,M., Parkin,N. and Varmus,H.E. (1992) An RNA pseudoknot and an optimal heptameric shift site are required for highly efficient ribosomal frameshifting on a retroviral messenger RNA. *Proc. Natl Acad. Sci. USA*, **89**, 713–717.
7. Dulude,D., Baril,M. and Brakier-Gingras,L. (2002) Characterization of the frameshift stimulatory signal controlling a programmed −1 ribosomal frameshift in the human immunodeficiency virus type 1. *Nucleic Acids Res.*, **30**, 5094–5102.
8. Dinman,J.D., Richter,S., Plant,E.P., Taylor,R.C., Hammell,A.B. and Rana,T.M. (2002) The frameshift signal of HIV-1 involves a potential intramolecular triplex RNA structure. *Proc. Natl Acad. Sci. USA*, **99**, 5331–5336.
9. Garcia,A., van Duin,J. and Pleij,C.W. (1993) Differential response to frameshift signals in eukaryotic and prokaryotic translational systems. *Nucleic Acids Res.*, **21**, 401–406.
10. Brierley,I., Digard,P. and Inglis,S.C. (1989) Characterization of an efficient coronavirus ribosomal frameshifting signal: requirement for an RNA pseudoknot. *Cell*, **57**, 537–547.
11. Giedroc,D.P., Theimer,C.A. and Nixon,P.L. (2000) Structure, stability and function of RNA pseudoknots involved in stimulating ribosomal frameshifting. *J. Mol. Biol.*, **298**, 167–185.
12. Stahl,G., McCarty,G.P. and Farabaugh,P.J. (2002) Ribosome structure: revisiting the connection between translational accuracy and unconventional decoding. *Trends Biochem. Sci.*, **27**, 178–183.
13. Plant,E.P., Jacobs,K.L., Harger,J.W., Meskauskas,A., Jacobs,J.L., Baxter,J.L., Petrov,A.N. and Dinman,J.D. (2003) The 9-A solution: how mRNA pseudoknots promote efficient programmed −1 ribosomal frameshifting. *RNA*, **9**, 168–174.
14. Bekaert,M., Bidou,L., Denise,A., Duchateau-Nguyen,G., Forest,J.P., Froidevaux,C., Hatin,I., Rousset,J.P. and Termier,M. (2003) Towards a computational model for −1 eukaryotic frameshifting sites. *Bioinformatics*, **19**, 327–335.
15. Bekaert,M. and Rousset,J.P. (2005) An extended signal involved in eukaryotic −1 frameshifting operates through modification of the E site tRNA. *Mol. Cell*, **17**, 61–68.
16. Lee,S.I., Umen,J.G. and Varmus,H.E. (1995) A genetic screen identifies cellular factors involved in retroviral −1 frameshifting. *Proc. Natl Acad. Sci. USA*, **92**, 6587–6591.
17. Peltz,S.W., Hammell,A.B., Cui,Y., Yasenchak,J., Puljanowski,L. and Dinman,J.D. (1999) Ribosomal protein L3 mutants alter translational fidelity and promote rapid loss of the yeast killer virus. *Mol. Cell. Biol.*, **19**, 384–391.
18. Donnelly,C.A., Ghani,A.C., Leung,G.M., Hedley,A.J., Fraser,C., Riley,S., Abu-Raddad,L.J., Ho,L.M., Thach,T.Q., Chau,P. *et al.* (2003) Epidemiological determinants of spread of causal agent of severe acute respiratory syndrome in Hong Kong. *Lancet*, **361**, 1761–1766.
19. Ksiazek,T.G., Erdman,D., Goldsmith,C.S., Zaki,S.R., Peret,T., Emery,S., Tong,S., Urbani,C., Comer,J.A., Lim,W. *et al.* (2003) A novel coronavirus associated with severe acute respiratory syndrome. *N. Engl. J. Med.*, **348**, 1953–1966.
20. Rota,P.A., Oberste,M.S., Monroe,S.S., Nix,W.A., Campagnoli,R., Icenogle,J.P., Penaranda,S., Bankamp,B., Maher,K., Chen,M.H. *et al.* (2003) Characterization of a novel coronavirus associated with severe acute respiratory syndrome. *Science*, **300**, 1394–1399.
21. Grentzmann,G., Ingram,J.A., Kelly,P.J., Gesteland,R.F. and Atkins,J.F. (1998) A dual-luciferase reporter system for studying recoding signals. *RNA*, **4**, 479–486.
22. Horton,R.M., Cai,Z.L., Ho,S.N. and Pease,L.R. (1990) Gene splicing by overlap extension: tailor-made genes using the polymerase chain reaction. *Biotechniques*, **8**, 528–535.
23. Ramos,F.D., Carrasco,M., Doyle,T. and Brierley,I. (2004) Programmed −1 ribosomal frameshifting in the SARS coronavirus. *Biochem. Soc. Trans.*, **32**, 1081–1083.
24. Baranov,P.V., Henderson,C.M., Anderson,C.B., Gesteland,R.F., Atkins,J.F. and Howard,M.T. (2005) Programmed ribosomal frameshifting in decoding the SARS-CoV genome. *Virology*, **332**, 498–510.
25. Napthine,S., Liphardt,J., Bloys,A., Routledge,S. and Brierley,I. (1999) The role of RNA pseudoknot stem 1 length in the promotion of efficient −1 ribosomal frameshifting. *J. Mol. Biol.*, **288**, 305–320.
26. Thiel,V., Ivanov,K.A., Putics,A., Hertzig,T., Schelle,B., Bayer,S., Weissbrich,B., Snijder,E.J., Rabenau,H., Doerr,H.W. *et al.* (2003) Mechanisms and enzymes involved in SARS coronavirus genome expression. *J. Gen. Virol.*, **84**, 2305–2315.
27. Mathews,D.H., Disney,M.D., Childs,J.L., Schroeder,S.J., Zuker,M. and Turner,D.H. (2004) Incorporating chemical modification constraints into a dynamic programming algorithm for prediction of RNA secondary structure. *Proc. Natl Acad. Sci. USA*, **101**, 7287–7292.
28. Shen,L.X. and Tinoco,I.,Jr (1995) The structure of an RNA pseudoknot that causes efficient frameshifting in mouse mammary tumor virus. *J. Mol. Biol.*, **247**, 963–978.
29. Chen,X., Chamorro,M., Lee,S.I., Shen,L.X., Hines,J.V., Tinoco,I.,Jr and Varmus,H.E. (1995) Structural and functional studies of retroviral RNA pseudoknots involved in ribosomal frameshifting: nucleotides at the junction of the two stems are important for efficient ribosomal frameshifting. *EMBO J.*, **14**, 842–852.
30. Kang,H. and Tinoco,I.,Jr (1997) A mutant RNA pseudoknot that promotes ribosomal frameshifting in mouse mammary tumor virus. *Nucleic Acids Res.*, **25**, 1943–1949.
31. Chen,X., Kang,H., Shen,L.X., Chamorro,M., Varmus,H.E. and Tinoco,I.,Jr (1996) A characteristic bent conformation of RNA pseudoknots promotes −1 frameshifting during translation of retroviral RNA. *J. Mol. Biol.*, **260**, 479–483.
32. Kontos,H., Napthine,S. and Brierley,I. (2001) Ribosomal pausing at a frameshifter RNA pseudoknot is sensitive to reading phase but shows little correlation with frameshift efficiency. *Mol. Cell Biol.*, **21**, 8657–8670.
33. Eleouet,J.F., Rasschaert,D., Lambert,P., Levy,L., Vende,P. and Laude,H. (1995) Complete sequence (20 kilobases) of the polyprotein-encoding gene 1 of transmissible gastroenteritis virus. *Virology*, **206**, 817–822.
34. Herold,J. and Siddell,S.G. (1993) An 'elaborated' pseudoknot is required for high frequency frameshifting during translation of HCV 229E polymerase mRNA. *Nucleic Acids Res.*, **21**, 5838–5842.
35. Su,L., Chen,L., Egli,M., Berger,J.M. and Rich,A. (1999) Minor groove RNA triplex in the crystal structure of a ribosomal frameshifting viral pseudoknot. *Nat. Struct. Biol.*, **6**, 285–292.
36. Kim,Y.G., Su,L., Maas,S., O'Neill,A. and Rich,A. (1999) Specific mutations in a viral RNA pseudoknot drastically change ribosomal frameshifting efficiency. *Proc. Natl Acad. Sci. USA*, **96**, 14234–14239.
37. Kim,Y.G., Maas,S. and Rich,A. (2001) Comparative mutational analysis of *cis*-acting RNA signals for translational frameshifting in HIV-1 and HTLV-2. *Nucleic Acids Res.*, **29**, 1125–1131.
38. Barry,J.K. and Miller,W.A. (2002) A −1 ribosomal frameshift element that requires base pairing across four kilobases suggests a mechanism of regulating ribosome and replicase traffic on a viral RNA. *Proc. Natl Acad. Sci. USA*, **99**, 11133–11138.